Atmos. Chem. Phys., 14, 2509–2524, 2014
www.atmos-chem-phys.net/14/2509/2014/
doi:10.5194/acp-14-2509-2014

Atmospheric Chemistry and Physics Open Access

Space-based observations of fire NO_x emission coefficients: a global biome-scale comparison

A. K. Mebust[1] **and R. C. Cohen**[1,2]

[1]Department of Chemistry, University of California at Berkeley, Berkeley, California, USA
[2]Department of Earth and Planetary Science, University of California at Berkeley, Berkeley, California, USA

Correspondence to: R. C. Cohen (rccohen@berkeley.edu)

Received: 22 July 2013 – Published in Atmos. Chem. Phys. Discuss.: 22 August 2013
Revised: 16 January 2014 – Accepted: 28 January 2014 – Published: 11 March 2014

Abstract. Biomass burning represents both a significant and highly variable source of NO_x to the atmosphere. This variability stems from both the episodic nature of fires, and from fire conditions such as the modified combustion efficiency of the fire, the nitrogen content of the fuel and possibly other factors that have not been identified or evaluated by comparison with observations. Satellite instruments offer an opportunity to observe emissions from wildfires, providing a large suite of measurements which allow us to study mean behavior and variability on the regional scale in a statistically rigorous manner. Here we use space-based measurements of fire radiative power from the Moderate Resolution Imaging Spectroradiometer in combination with NO_2 tropospheric column densities from the Ozone Monitoring Instrument to measure mean emission coefficients (ECs in g NO MJ^{-1}) from fires for global biomes, and across a wide range of smaller-scale ecoregions, defined as spatially-distinct clusters of fires with similar fuel type. Mean ECs for all biomes fall between 0.250–0.362 g NO MJ^{-1}, a range that is smaller than found in previous studies of biome-scale emission factors. The majority of ecoregion ECs fall within or near this range, implying that under most conditions, mean fire emissions of NO_x per unit energy are similar between different regions regardless of fuel type or spatial variability. In contrast to these similarities, we find that about 24 % of individual ecoregion ECs deviate significantly (with 95 % confidence) from the mean EC for the associated biome, and a similar number of ecoregion ECs falls outside the range of all mean biome ECs, implying that there are some regions where fuel type-specific global emission parameterizations fail to capture local fire NO_x emissions.

1 Introduction

Biomass burning emissions induce a variety of effects to climate and air quality. They impact the global radiative budget directly by absorbing or reflecting incoming radiation, e.g. CO_2 and aerosols, and/or indirectly by influencing the chemistry or physics of climate forcers, e.g. nitrogen oxides ($NO_x = NO + NO_2$) and CO acting as ozone (O_3) precursors or aerosol indirect impacts on clouds (Bowman et al., 2009; Fiore et al., 2012; Jaffe and Wigder, 2012). O_3 and aerosols also have negative health impacts, especially at high concentrations. Understanding, quantifying and mitigating these effects requires an understanding of both the magnitude of the emissions, as well as their variability across a range of spatial and temporal scales.

Current models of fire emissions rely on a biomass-burned approach: to estimate the mass of a compound emitted, an emission factor (EF in g kg^{-1} biomass burned) derived from in situ measurements of smoke is multiplied by an estimate of the total biomass burned, often calculated as the product of other factors, e.g. burn area, fuel loading, combustion completeness (Andreae and Merlet, 2001; Wiedinmyer et al., 2006; van der Werf et al., 2010). This strategy has weaknesses, as the uncertainty in biomass burned for a particular fire is high, and even aggregate estimates at lower spatial and temporal resolution can have significant biases (van der Werf et al., 2010; Granier et al., 2011). Additionally, measured EFs vary greatly between individual fires due to differences in fire conditions, e.g. fuel type, structure, moisture, etc. (Andreae and Merlet, 2001; Korontzi et al., 2003; van Leeuwen and van der Werf, 2011; van Leeuwen et al., 2013). In this work, we focus on emissions of NO_x, which

are produced in wildfires as the result of oxidative combustion of nitrogen (N) contained in the biomass (Andreae and Merlet, 2001). Measured NO_x EFs for fires are generally considered to be positively correlated with modified combustion efficiency (MCE) and fuel N content (e.g. Lacaux et al., 1996; Battye and Battye, 2002). A high MCE indicates a greater contribution of higher-temperature flaming combustion which is thought to oxidize the N more effectively, while high fuel N provides a larger source of N to ultimately be oxidized to NO_x (Andreae and Merlet, 2001). However, observational evidence confirming these effects is limited, leading to a lack of understanding regarding the extent of these relationships. Observed correlations between NO_x EFs and MCE are typically poor (e.g. Battye and Battye, 2002; Yokelson et al., 2011), and fuel nitrogen content is rarely quantified. Models of fire NO_x emissions typically use EFs for a few (3–7) fuel types, based on averages of EFs measured for fires of each particular fuel type (e.g. Andreae and Merlet, 2001; Hoelzemann et al., 2004; van der Werf et al., 2010; Akagi et al., 2011). The number of fires from which each EF is derived ranges from a handful (3–5) to tens or perhaps even hundreds, depending on the fuel type and the emitted species in question. However, even when EFs are derived from large numbers of fires, these observations come from only a few targeted measurement campaigns that sample many fires with fuels comprised of a relatively small range of plant species and over a short temporal span (e.g. Akagi et al., 2011). This raises the question of whether the observations are representative of variations in emissions that would be observed under a more spatially and temporally comprehensive sampling strategy that incorporates spatially distinct fire regimes with the same fuel type and covers seasonal and interannual variations in rainfall, wind speed and other climatic conditions.

Several satellite instruments measure fire-related properties, providing data that span the globe, sample throughout the year, and include many fires in each region, allowing for statistical evaluation of variance in emissions and reducing the potential for bias due to an unrepresentative sample. Deriving an EF from satellite observations, however, is challenging due to the difficulty in estimating biomass burned in the fire and connecting that information to instantaneous measurements of atmospheric composition. Instead, methods for estimating the mass of a pollutant emitted per unit radiative energy released from the fire – a value we define as the emission coefficient (EC) to distinguish it from the EF – have been developed (Ichoku and Kaufman, 2005; Jordan et al., 2008; Vermote et al., 2009; Mebust et al., 2011; Mebust and Cohen, 2013). The idea for an EC was born out of laboratory work that established a linear relationship between the amount of energy released by a fire and the total biomass burned, suggesting that (a) an energy-based parameterization is a logical alternative to a mass-based one, and (b) measured ECs should be proportional to EFs (Wooster, 2002; Wooster et al., 2005; Freeborn et al., 2008). ECs provide a straightforward way to estimate EFs from satellite observations because measurements of fire radiative power (FRP) are made daily with near-global coverage from the two Moderate Resolution Imaging Spectroradiometer (MODIS) instruments, allowing for near-simultaneous estimation of energy and pollutant emissions for any species measured from space near the MODIS overpass times.

In two previous papers, we developed a method to combine global observations of FRP from MODIS with NO_2 tropospheric column density measurements from the Ozone Monitoring Instrument (OMI) to calculate ECs for NO_x and assessed the method as applied to fires in California and Nevada, and also examined seasonal variability in ECs in African savannas (Mebust et al., 2011; Mebust and Cohen, 2013). Here we adapt this method to provide a global picture of variations in NO_x emissions. We calculate ECs for several global biomes and for different ecoregions within these biomes, and describe how these ECs compare to each other and to EFs reported in previous studies.

2 Data

This analysis incorporates information from OMI, MODIS, a climate classification system, and the Climate Forecast System Reanalysis (CFSR) and Version 2 Reforecast (CFSv2). We use global observations from years 2005–2011.

2.1 OMI

OMI is a nadir-viewing spectrometer onboard the polar-orbiting EOS-Aura satellite, with an equatorial overpass time of $\sim$ 13:45 (local time). OMI measures the solar irradiance and backscatter radiance from Earth at UV and visible wavelengths (270–500 nm with 0.5 nm resolution) to derive column densities for several trace gases. We use tropospheric vertical NO_2 column densities obtained from the OMI NO_2 standard product (OMNO2, Level 2, Version 2.1, Collection 3). The retrieval process for these columns is described in detail elsewhere (Bucsela et al., 2013); briefly, slant NO_2 columns are derived using differential optical absorption spectroscopy (DOAS), separated into stratospheric and tropospheric components, and converted to vertical column densities using an air mass factor, which is derived from several parameters including terrain reflectivity and height and an estimated NO_2 vertical profile. The spatial footprint is $13 \times 24\,km^2$ at nadir. We use data from the inner 40 (of 60) across-track pixels, omitting the low spatial resolution observations at the edge of the swath; resolution at the largest remaining pixels is approximately $15.5 \times 42\,km^2$. We also limit observations to those with a cloud fraction of less than 20 %, as pixels with a high cloud fraction have reduced sensitivity to NO_2 below the clouds (Boersma et al., 2002), and we reject all pixels affected by the row anomaly. Restrictions to cloud fraction (20–30 % cloud fraction, or 50–70 % radiance fraction) are generally accepted as good practice in studies of

OMI NO_2 columns when looking at surface emissions. Small differences in this value do not significantly affect the results presented here.

It is plausible that the a priori NO_2 vertical profile shapes used in the retrieval process might lead to a bias in measured NO_2 columns over smoke plumes. The OMNO2 standard product v2.1 uses GMI CTM monthly mean modeled NO_2 vertical profile shapes at $2^\circ \times 2.5^\circ$ (Bucsela et al., 2013). Previous work has identified a negative bias over persistent features smaller than this model resolution that results from the low spatial resolution of the estimated NO_2 profile. Specifically, Russell et al. (2011) developed a regional OMI NO_2 retrieval and found that urban NO_2 columns increased by 8 %, and this increase was primarily attributed to using WRF-Chem profiles at $4\,\mathrm{km} \times 4\,\mathrm{km}$ resolution as opposed to the lower resolution profiles in the NASA standard product v1.0. This is consistent with the observation by Boersma et al. (2011) that when near-surface NO_2 gradients were less strong, it resulted in a decrease in measured NO_2 for a different retrieval of OMI, because a larger fraction of NO_2 was distributed relatively higher in the atmosphere where the OMI instrument sensitivity is higher. Given that fires are episodic, heavy-emitting point sources in regions that are typically remote with few other NO_x emission sources, the assumed NO_2 vertical profile will have very little NO_2 distributed in the lowest layer as compared to the "true" NO_2 vertical profile over most fires. This difference will be much more pronounced than in an urban area where the assumed profile, while diluted over a large spatial scale, still represents some of the vertical gradient over a NO_x source, and thus we expect a much larger bias. The impact of high aerosol loading may also have an effect, as one study considered the effects of mixed and/or layered aerosol and NO_2 on the NO_2 retrieval and found that effects are theoretically small when NO_2 and aerosol are collocated but much larger if the aerosol is above or below the plume (Leitao et al., 2010). However, the importance of this effect to our work is uncertain, as it is expected that fresh smoke plumes will generally contain well-mixed NO_2 and aerosol. The potential magnitude of this effect is also unknown and estimating this magnitude is beyond the scope of this work. Regardless, there is a theoretical basis for a low bias in OMI NO_2 measurements over smoke plumes.

In Mebust et al. (2011) we found that EFs derived from measurements of MODIS FRP and OMI NO_2 were lower than reference EFs by a factor of approximately 2–5 (depending on the reference EF). We performed a comprehensive quantitative assessment of potential error sources, including the assumed NO_x lifetime, assumed $NO_2 : NO_x$ ratio, value used to convert from energy released to biomass burned, diurnal behavior of FRP, choice of wind height, screening of FRP by clouds and/or canopy cover, and possible diurnal behavior of emission factors. We found that, with the exception of any bias in OMI NO_2 for which we could not provide a quantitative estimate, the sources with an expected positive bias were balanced by sources with an expected negative bias. Thus, the source of the observed discrepancy is not understood, although it potentially stems in part from the aforementioned low bias in OMI NO_2 over fires. However, we do not believe it varies in a statistically representative ensemble of fires, and thus relative differences in ECs are believed to be reliable. A more comprehensive and quantitative assessment of errors can be found in Mebust et al. (2011).

2.2 MODIS

MODIS instruments operate on NASA's Aqua and Terra satellites. MODIS measures spectral radiance in 36 bands which cover visible and IR wavelengths. We use the Thermal Anomalies product (MYD14, Level 2, Collection 5) and the Land Cover product (MCD12Q1, Level 3, Collection 5.1). We only include fires detected by the Aqua MODIS instrument during daytime, as this allows near-coincident measurement of fires and NO_2 column densities. The Aqua equatorial overpass time is $\sim$ 13:30 (local time), meaning OMI and MODIS measurements are typically made ~ 15 min apart. Fires are detected using the 4 µm and 11 µm bands; pixels with elevated radiance in these bands as compared to surrounding pixels are labeled as containing fire. The spatial resolution of the bands is $1 \times 1\,\mathrm{km}^2$, but the algorithm is sensitive enough to detect fires as small as $100\,\mathrm{m}^2$. An estimate of pixel FRP is derived from the 4 µm brightness temperature. Further details on the fire detection and FRP estimation algorithms are discussed elsewhere (Kaufman et al., 1998; Justice et al., 2002; Giglio et al., 2003)

It has been suggested that there exists a low bias in MODIS FRP resulting from reduced sensitivity to radiance under conditions where fires are too small to be detected, obscured by clouds or canopy cover, or burning below ground (e.g. Wooster et al., 2003; Boschetti and Roy, 2009; Vermote et al., 2009; Freeborn et al., 2011). In this analysis we minimize most of these biases because we use only detected fires and compare with NO_2 columns directly over the source. In most of these cases, the percentage of undetected FRP due to undetected or cloud-obscured actively burning locations is likely small. In Mebust et al. (2011), we determined that the magnitude of this bias was on the order of 15–30 % and that its effect on the derived ECs is counteracted by other biases. However, to the extent that our analysis considers relative differences in ECs, it may be sensitive to canopy effects or underground burning because these effects may vary in magnitude between different biomes. A low bias in FRP in particular biomes would elevate reported EC values in those biomes.

Land cover classifications are assigned to $500 \times 500\,\mathrm{m}^2$ pixels using the International Geosphere-Biosphere Programme (IGBP) classification (Friedl et al., 2010). We assume that land cover in 2011 is the same as in 2010 because at the time of this analysis, the land cover product was only available for years 2005–2010. Using comparisons of 2009

Table 1. Classification of IGBP classes to broad biome categories.

IGBP class	Biome category
Water	Not assigned
Evergreen needleleaf forest	Forest
Evergreen broadleaf forest	Forest
Deciduous needleleaf forest	Forest
Deciduous broadleaf forest	Forest
Mixed forest	Forest
Closed shrublands	Shrub
Open shrublands	Shrub
Woody savannas	Grass
Savannas	Grass
Grasslands	Grass
Permanent wetlands	Not assigned
Croplands	Agricultural
Urban and built-up	Not assigned
Cropland/natural vegetation mosaic	Not assigned
Snow and ice	Not assigned
Barren/sparsely vegetated	Not assigned

and 2010 land cover, we estimate that only about 10 % of 2011 observations will be assigned an incorrect biome due to this assumption, which amounts to about 0.5 % of all observations. The IGBP classification scheme provides 17 different categorizations of land type; we assign many of these categories to biome categories as shown in Table 1, but occasionally use the direct IGBP classifications.

2.3 Köppen-Geiger climate classification

Common EF schemes distinguish between tropical, temperate, and occasionally boreal forests (Andreae and Merlet, 2001; Hoelzemann et al., 2004; van der Werf et al., 2010; Akagi et al., 2011); to identify these distinct forest types we use the Köppen–Geiger global climate classification system at $0.5° \times 0.5°$ resolution (Kottek et al., 2006). This dataset classifies climate as one of five main climate types ("equatorial," "arid," "warm temperature," "snow," "polar"), with additional sub-classifications related to precipitation and temperature. We classify forests as "tropical" if they are found in "equatorial" climates, "temperate" if they are found in "arid" or "warm temperate" climates, and "boreal" if they are found in "snow" or "polar" climates. We also use subclassifications of the "equatorial" regime ("fully humid", "monsoonal" and "winter-dry") to separately examine differences in tropical evergreen vs. tropical dry deforestation.

2.4 CFSR, CFSv2

The CFSR is a global reanalysis and forecast for years from 1979 through 2010; CFSR was extended starting in 2011 using CFSv2 and continues as an operational real-time product (Saha et al., 2010, 2014). Wind fields used in this work are from the 850 hPa vertical level (corresponding to approximately 1.5 km altitude) and are available at $0.5° \times 0.5°$ resolution hourly. The reanalysis is performed with 6 h time steps and this is coupled with forecasts to provide output for every hour.

3 Methodology

We build on the methodology described in Mebust et al. (2011), which was adapted from Ichoku and Kaufman (2005). All fire pixels detected by the Aqua MODIS instrument daytime overpasses during 2005–2011 are assigned a land type using the MODIS land cover product for the appropriate year (or 2010 for fire pixels detected in 2011) and matched with OMI pixels coincident in space and from the same orbit (ranging from 7–22 min apart). OMI pixels that contain fire pixels with FRP above 250 MW are aggregated using a sorting algorithm such that adjacent OMI pixels are analyzed as a single fire "event". We note that Mebust et al. (2011) included OMI pixels containing less than 250 MW of FRP. Globally, we observed that there are many regions where fires occur more densely than in California and Nevada. Here, we chose the 250 MW criterion because we determined through testing that it was the minimum possible cutoff at which most pixels in these fire-dense regions did not aggregate into extremely large groups; we also calculated that under standard conditions of wind speed and predicted emission rates, the change in column density of NO_2 over an individual fire with FRP equal to 250 MW would generally be below the detection limit of OMI. To further ensure removal of data that cannot be attributed to an individual fire, we did not analyze any fire events that were greater in size than 3 OMI pixels in the along-track dimension or 2 OMI pixels in the across-track direction. Events greater than this size were typically aggregates of multiple small fires (e.g. several nearby agricultural fires) rather than individual fires. This restriction removed fewer than 1 % of observations.

The total mass of NO_2 emitted by each fire was calculated using the total area of OMI pixels in the event and the column density of NO_2 over the fire after subtracting a background column density, calculated using fire-free OMI observations in the same location covering a period of 60 days before and 60 days after the fire. Events for which there were less than 10 valid background observations were considered to have a poorly characterized background column and were not analyzed further. Tests in Mebust and Cohen (2013) established that deriving the background from a smaller range of observations (e.g. 30 days before and 30 days after) reduced the observational sample size but did not otherwise affect the results. The time over which the observed NO_2 was emitted, the "clear time", was then calculated using the wind speed and direction near the fire, the OMI pixel edges, and the center of the fire, calculated as the mean of fire pixel locations weighted by pixel FRP. Dividing the mass of NO_2 emitted by the clear time yields the mass emission rate (MER), or rate

Table 2. Summary of calculated emission coefficients and emission factors for NO_x as NO.

Fuel type	NO_x EC ($g\,MJ^{-1}$)[a]	NO_x EF ($g\,kg^{-1}$)[a,b]	N	R^2
Tropical forests	0.356 ± 0.044	0.87 ± 0.11	6266	0.307
Temperate forests	0.298 ± 0.019	0.727 ± 0.047	3417	0.293
Boreal forests	0.250 ± 0.033	0.609 ± 0.079	1633	0.308
Extratropical forests[c]	0.275 ± 0.020	0.670 ± 0.049	5050	0.298
Grasslands	0.362 ± 0.015	0.883 ± 0.037	73789	0.290
Shrublands	0.275 ± 0.030	0.671 ± 0.075	4764	0.439
Agriculture	0.266 ± 0.024	0.650 ± 0.061	4732	0.068

Uncertainty for ECs and EFs is given as the standard error of the EC (σ). [a] Assumes 75 % of NO_x is present as NO_2. [b] Calculated using a value of 0.41 kg MJ^{-1} (Vermote et al., 2009). [c] Extratropical forests include both boreal and temperate forests.

at which the fire is emitting NO_2 as observed by the satellite. This is not, however, the direct NO_2 EC from the fire, since the NO_2 observed by satellite is at photostationary state. We assume that at photostationary state, 75 % of NO_x is present as NO_2 to obtain the EC for NO_x. This assumption is consistent with previous in situ measurements which typically find that NO_2 constitutes 50–100 % of NO_x. Since we are concerned with relative comparisons of EFs, it is important to establish that this fraction will not vary significantly as a result of background ozone concentration. We estimate that the impact from this effect is small because our ECs scale by $(NO + NO_2) : NO_2$ rather than the direct ratio $NO : NO_2$, and calculate that factor-of-two differences in background ozone will result in < 20 % change to $(NO + NO_2) : NO_2$. In Mebust and Cohen (2013) we presented evidence that seasonal variations in NO_x ECs in African savannas were not primarily driven by changes in background ozone. For all ECs and EFs described in this work, the mass of NO_x is calculated as NO, a common practice for fire NO_x emissions.

Satellite observations of fire plumes inevitably contain a mix of fresh (immediately over the source) and aged (downwind) emissions. Although the OMI spatial resolution is relatively high, NO_x loss is fast enough (lifetime on the scale of hours) that significant loss of NO_x can occur by the time the plume reaches the edge of the OMI pixel. We correct for this effect using a 1-D model and 2 h lifetime assumption as described in Mebust et al. (2011). All data subsequently presented in this paper has been adjusted using this model and assumed lifetime.

To ensure the data is representative of emissions from fires, we remove points with high background column density (3.5×10^{15} molecules cm^{-2}), or either long (> 3 h) or short (< 15 min) clear times. Observations with a high background tend to yield higher uncertainty in calculated mass of NO_2 emitted by the fire; long clear times increase the likelihood that the fire violates the assumption that the fire properties have not changed significantly over the time of observation; and short clear times can result in an anomalously high (or negative) MER as the clear time appears in the denominator of the MER, amplifying uncertainty in the difference between the observed NO_2 column density over the fire and the background NO_2 column density. Approximately 30 % of observations are removed by these filters.

We present results for all fires of a particular fuel type across the globe (i.e. a "biome-scale" EC) and for spatially distinct clusters of fires of similar fuel types (i.e. an "ecoregion-scale" EC). We note that the phrase "fuel type" as used throughout this work is intended to distinguish across-biome variability in fuel composition (e.g. forest vs. grassland fuels), not within-biome variability in characteristics such as fuel moisture, relative contributions of leaf litter vs. woody materials, etc. Fire biomes are identified using primary land cover type (for all fires) and climate classifications (for forests). To be classified as a particular biome type, 75 % of FRP from a fire must come from fire pixels identified as that biome type. We use a spatial clustering method to further classify fires into ecoregions; fires of an individual fuel type (e.g forests) that occur within 250 km (100 km for grasses) of each other are grouped and each group is considered an ecoregion for the purpose of this analysis. ECs for both biomes and ecoregions are derived via linear regression with nonparametric bootstrap resampling using 5000 resamples (Efron and Tibshirani, 1986). The intercept is not forced through zero to account for any possible small bias in emission estimates from low-energy fires. Typically we require at least 100 observations to consider an EC adequately constrained. We also remove extreme high-weight points by removing all points that affect the fit by 100 % or more. There are only two ecoregions (and no biomes) that contain points that fall into this category; one ecoregion contained one such point and the other contained two.

4 Results

4.1 Biome-scale ECs

Figure 1 shows a map of all fires used to derive ECs. Fires are labeled as "other" if at least 75 % of FRP came from fire pixels not assigned to a biome type (see Table 1), or as "mixed" if they fail to meet the 75 % criteria for any

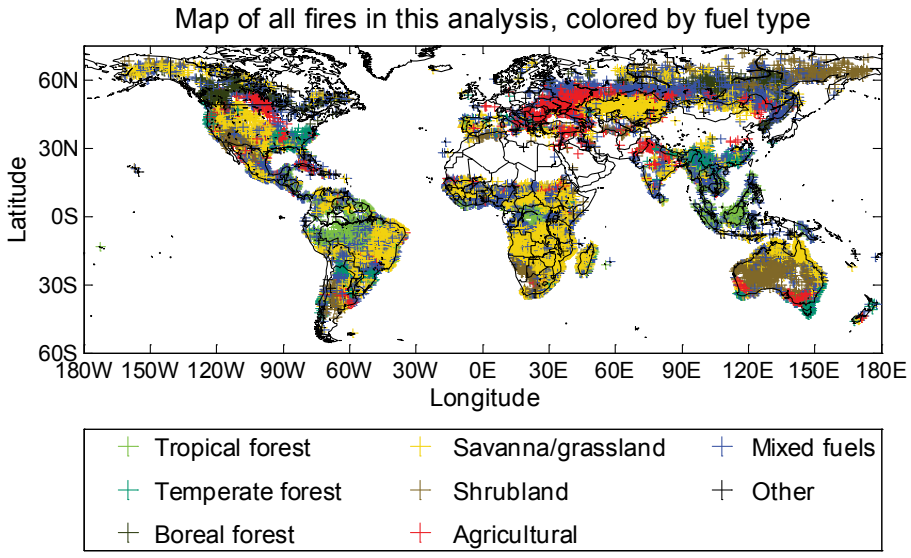

Fig. 1. Map of fires used in this analysis. Color indicates fuel type as determined using land cover and climatology. Fires were identified as having a particular fuel if greater than 75 % of measured FRP for that fire came from fire pixels of a single fuel type; fires not meeting this criterion are designated "mixed fuels". Fires are labeled as "other" if at least 75 % of measured FRP came from fire pixels not assigned a biome type.

individual biome type. We derive ECs for seven different biomes, keeping in mind that similar classifications are used in most fire emission modeling frameworks (e.g. GFED). The results are presented in Table 2, along with an estimate for conversion to an EF, the number of fires (N), and the coefficient of determination (R^2). Calculated ECs fall between 0.250–0.362 g NO MJ^{-1}; the lowest calculated EC (boreal forest) is ∼ 70 % of the highest calculated EC (grasslands).

NO_x EFs for wildfires are inherently variable, and thus it is important to distinguish between this variability and the confidence in the mean estimate of an EF for a group of fires. Traditional in situ measurement campaigns generally include the standard deviation of any calculated EF to provide an estimate of the variability between fires. The standard deviation conflates both inherent variability and also measurement uncertainty; however, for in situ measurements of fire emissions the measurement uncertainty tends to be low and thus the standard deviation primarily reflects the variability. These standard deviations tend to be large relative to the value of the EF due to this inherent large variability. An alternative metric, the standard error, indicates the confidence in the mean value rather than this inherent variability, and is valuable when attempting to assess uncertainties associated with emission estimates for aggregates of several fires. The standard error is related to the standard deviation but also depends on the number of observations – as the sample size of observations increases, the standard error decreases while the standard deviation does not. A major strength of our analysis is in the large number of observations we are able to analyze; however, each individual measurement in our analysis is associated with a higher uncertainty than in situ measurements. This uncertainty in individual measurements is large enough that estimates of variability in our analysis necessarily conflate the inherent natural variability and also the measurement uncertainty. Therefore, for the biome- and ecoregion-scale ECs reported in this work, we provide an estimate of the standard error only, noting that there remains a large variability in ECs for individual fires.

For an example of this inherent variability (with contributions from individual measurement uncertainty), we calculate ECs directly (dividing MER by FRP) for fires of all fuel types with high FRP (> 5000 MJ s^{-1}). The distribution, with both arithmetic and geometric mean and standard deviation, of the directly-calculated ECs is shown in Fig. 2. The arithmetic standard deviation of ECs is 72 % of the arithmetic mean. However, the distribution is not normal, limiting the value of arithmetic statistics. A log-normal distribution and geometric statistics offer a better description of the observations. The geometric mean for a log-normal distribution is equal to the median; the geometric standard deviation is a multiplicative factor rather than an additive one. In this case, a geometric standard deviation of ∼ 2 indicates that approximately 68 % of observations are contained between one-half and twice the geometric mean. Unfortunately, this kind of analysis requires a large number of high-FRP fires so it cannot be used to compare variability between biomes and ecoregions. Another way to highlight the natural variability of ECs between individual fires is to consider the R^2 value, which is also the fraction of explained variance. An R^2 of ∼ 0.3 (as observed in the case of most of our biome-scale ECs) indicates that about 70 % of the variance is unexplained by a linear relationship between FRP and MER.

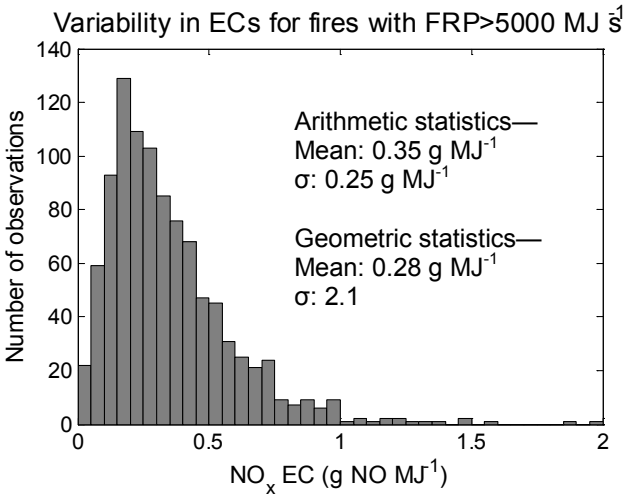

Fig. 2. Histogram of ECs of NO_x (as NO) measured for fires with FRP above 5000 MJ s^{-1}. ECs were calculated by dividing the MER by FRP for individual fires.

Despite the large variance, however, most of our ECs have a relatively low standard error, or estimate of the uncertainty in the mean EC (15 % or lower). As previously mentioned, this is because of the large number of observations that factor into each EC. One advantage of the nonparametric bootstrap resampling method we use to calculate each EC is that it provides a direct estimate of this distribution of variability in the best fit parameter via the distribution of bootstrap resamples. Therefore we can estimate the standard error in our ECs by calculating the standard deviation of the bootstrap resamples. We use this method to provide the standard error of all ECs presented in this work. The bootstrap resamples are generally normally distributed, so we provide arithmetic standard deviations as our estimate of the standard error.

4.2 Spatial variability within biomes

Within each biome there are several spatially distinct ecoregions. Our analysis identified 42 separate ecoregions. Three of the forest ecoregions spanned multiple biomes (e.g. tropical and temperate forests) so we calculate two ECs for each of these three ecoregions; thus we calculate 45 ecoregion-scale ECs in all. Maps of ecoregions and corresponding ECs are shown in Figs. 3–6; ECs, R^2 and N for each ecoregion are available in tables in the Supplement. We also calculate p values, the probability that each ecoregion EC is the same as the mean biome EC, for statistical testing directly using bootstrap distributions of the difference between each ecoregion EC and the mean EC for that biome. We find that most (34 out of 45, or $\sim$ 75 %) ecoregion ECs are not significantly different than the mean biome EC at the 0.05 level. However, there are ecoregions with significantly different ECs in all biomes. We include the p value in the supplementary tables for these cases. When differences between ecoregion and mean biome ECs are statistically significant, they tend to be large, with most differences ranging from 50 % to more than a factor of 2.

4.2.1 Forests

Figure 3 shows a map of all forest ecoregions containing more than 100 separate observations and ECs for those ecoregions. Fires from clusters with fewer than 100 observations are shown in black. ECs are calculated separately for each biome category (e.g. tropical vs. temperate forest) and biomes are indicated by marker shape. The range of mean biome ECs for all biomes is indicated in grey. We find that one of six tropical forest ecoregion ECs is significantly different from the mean tropical forest EC (Region B); similarly, one of six temperate forest ecoregion ECs is significantly different from the mean temperate forest EC (Region G). One of two boreal forest ecoregion ECs is different from the mean boreal forest EC (Region K). Correlation coefficients (R^2) for each ecoregion range between 0.1 and 0.5 (see Supplement).

4.2.2 Grasses

Results for grass fire ecoregions are found in Fig. 4. These ecoregion ECs are the most variable of all the biomes; six of the seventeen ecoregions have ECs that are significantly different from the mean grassland EC (Regions L, P, R, X, Y, and Z). In these ecoregions, ECs range from as large as 0.95 to as small as 0.187 g NO MJ^{-1}. However, ECs in the remaining ecoregions are all within 30 % of the mean grassland EC. Correlation coefficients (R^2) for each ecoregion range from 0.1 to 0.7; seven of the seventeen ecoregions have R^2 greater than 0.4. Three of those have ECs that differ significantly from the mean (Regions X, Y and Z).

4.2.3 Shrubs

The shrubland biome is not considered in most global treatments of fire NO_x emissions, likely because there are few measurements of shrub EFs and shrub fires generally do not make up a large portion of the global biomass consumed by fire. These fires are (presumably) partitioned into other biome categories. Our mean biome EC for shrubs falls within the range of other mean biome ECs, suggesting that treating shrub fires as grass or forest fires would not cause a large bias in global total fire emissions. Results from our shrub ecoregion analysis are presented in Fig. 5. The range of variation is smaller than in other biomes, although one of five ecoregions is statistically significantly different from the mean shrub EC (Region DD). Correlation coefficients for these ecoregions are generally much higher than for ecoregions in other biomes, ranging from 0.3 to 0.7 with four of five regions having $R^2 \sim 0.4$ or above. This may be due to better consistency in emission conditions as a result of the smaller size of the shrub regions vs. grass or forest regions

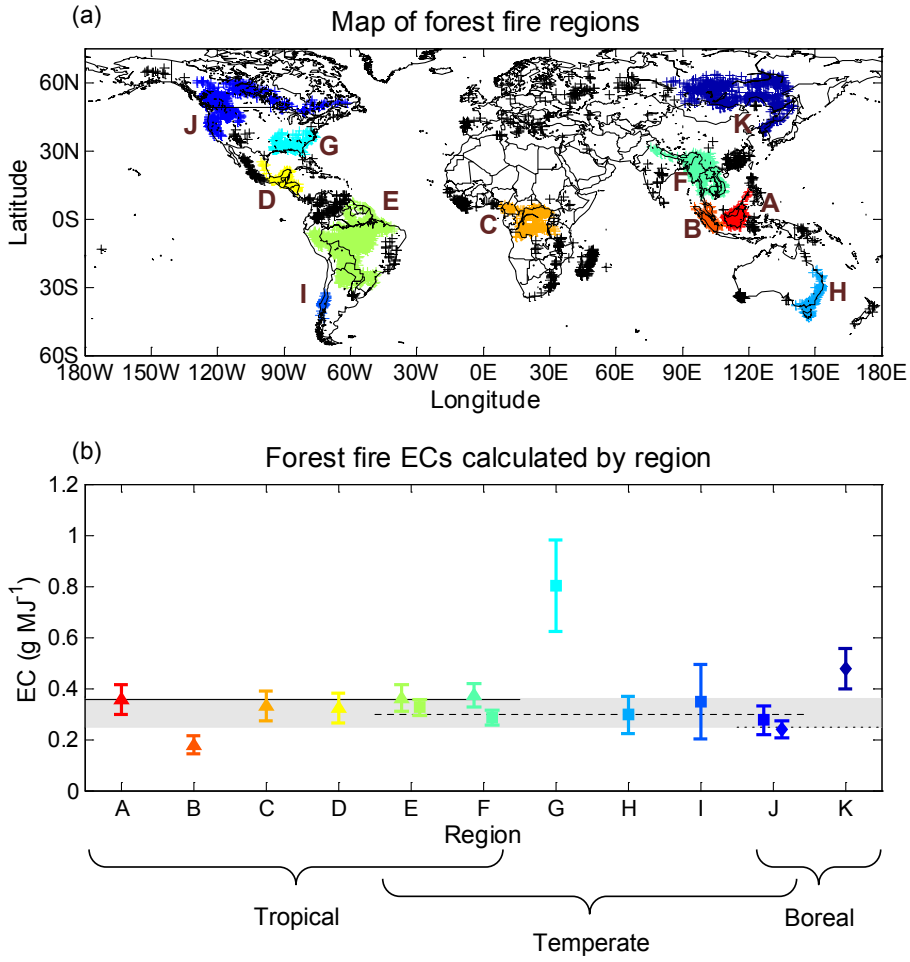

Fig. 3. A map of forest fire regions determined by a clustering analysis **(a)** and ECs calculated individually for each region **(b)**. In **(a)**, black markers identify forest fires belonging to clusters with less than 100 observations. In **(b)**, marker shapes are used to identify biomes for each EC, determined via climate classifications: triangles indicate tropical, squares indicate temperate, and diamonds indicate boreal forests. In regions where there is adequate sampling of more than one biome type, ECs are calculated for both biomes (e.g. Region E). The tropical (solid), temperate (dashed) and boreal (dotted) forest mean biome ECs are indicated by the black horizontal lines. The range of all mean biome ECs (as presented in Table 2) is indicated in grey.

and/or of the greater number of highly energetic fires as a percent of observations (> 10 % of observations have FRP above 2000 MJ s^{-1} for shrub fires, as opposed to less than 10 % for grass and forest fires). The reasons for higher FRP in shrub biomes is not clear, but may be related to the higher fuel loading as compared to grass fires, and the potentially higher temperature combustion and/or faster rate of spread as compared to forest fires.

4.2.4 Agriculture

Results for agricultural fires are presented in Fig. 6. Fire emissions of NO_x from this biome are perhaps the hardest to characterize, because these controlled fires are usually small. This is reflected in the relatively larger uncertainties (see Fig. 6b) and also in much lower correlation coefficients; R^2 is below 0.15 for all but one of the 9 crop regions shown below. Only one of the nine ecoregion ECs is statistically significantly different from the mean agricultural EC (Region NN); however, that may partly be due to the higher uncertainties in ECs for this crop type. Using a harvested crop area dataset (Monfreda et al., 2008), we identify the main crop type for most regions to be wheat, except Region HH (sorghum) and Regions KK and LL (soybeans). There is no obvious relationship between crop type and EC.

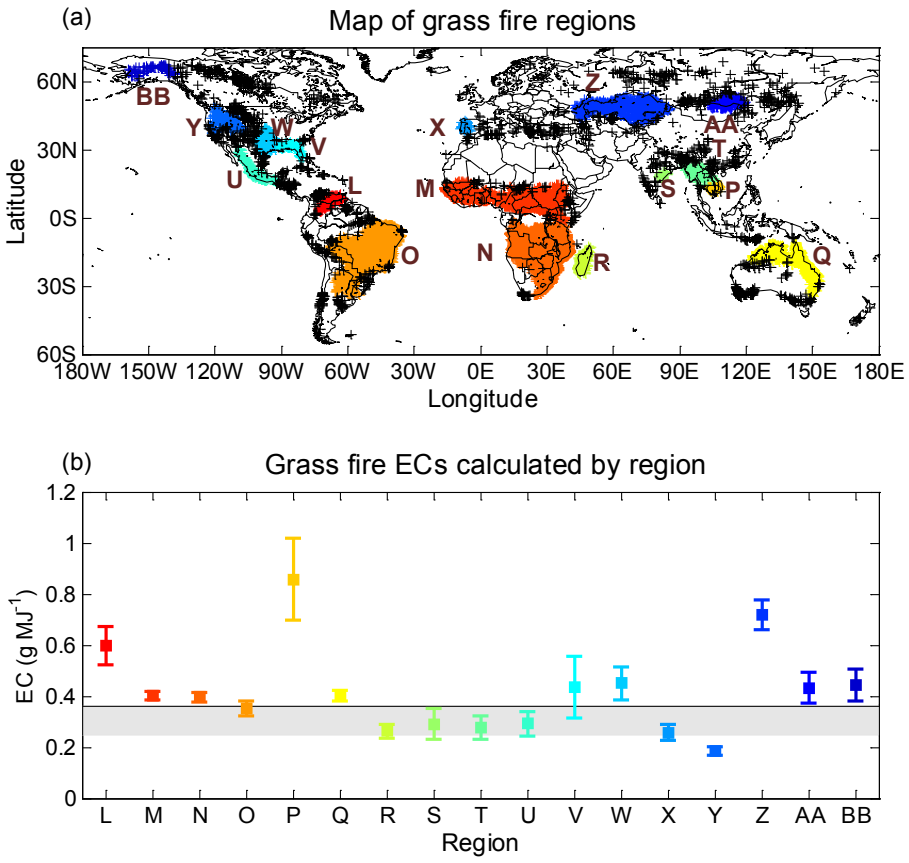

Fig. 4. A map of grass fire regions determined by a clustering analysis **(a)** and ECs calculated individually for each region **(b)**. In **(a)**, black markers identify grass fires belonging to clusters with less than 100 observations. In **(b)**, the mean grassland biome EC is indicated by the black line, while the range of all mean biome ECs (as presented in Table 2) is indicated in grey.

5 Discussion

5.1 Biome- and ecoregion-scale similarities and differences

Broadly, the ECs presented here suggest that mean fire behavior is similar regardless of biome or ecoregion. We find that 75 % of ecoregion ECs are not significantly different from the corresponding biome-scale EC. These "biome-similar" ecoregion ECs fall within 32 % of the mean biome EC for all biomes except agriculture; within some biomes, the difference between the largest and smallest "biome-similar" ecoregion ECs is as low as a few percent. Differences in the agricultural biome are larger partly because of larger uncertainties in the derived ECs. As previously noted, biome-scale ECs themselves cover a relatively narrow range (the lowest value is ∼ 70 % of the highest value). We find that almost half of the ecoregion-scale ECs (21 out of 45) fall directly into this range, and for 9 more ecoregion-scale ECs the difference between the EC and this range is less than the standard error of the ecoregion-scale EC. However, there are several ecoregion-scale ECs that do not overlap this range within the ecoregion standard error of the EC, or even twice the ecoregion standard error of the EC. These ECs are generally substantially different (i.e. by 50 % or more) from the biome scale ECs. These differences suggest that emissions differ more with location than with fuel type, challenging the traditional model of emissions as fuel type-specific.

The number of observations within each ecoregion that deviate significantly from the mean biome ECs is large enough to confirm that these differences are statistically robust and not the product of an anomalously small sample size. The large differences in these ECs as compared to the mean biome EC will result in significant biases in emission estimates for these specific regions if the mean EC is used. The most notable of these is for boreal forest in Asia (Region K). Most conventional estimates of boreal forest NO_x EFs are derived from measurements of fires in North America; however, we find that ECs in boreal forest in Asia are fully twice those in North America (Region J). This is particularly important because emissions from boreal forest fires play an especially important role in global atmospheric composition and chemistry (Jacob et al., 2010; Simpson et al., 2011).

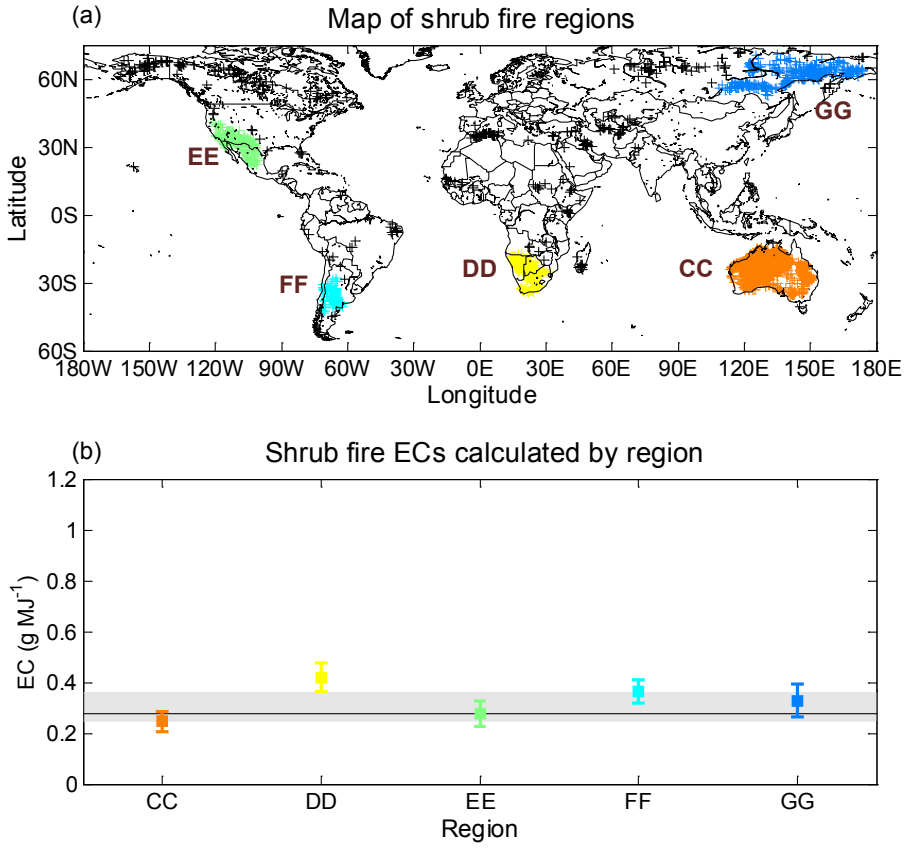

Fig. 5. A map of shrub fire regions determined by a clustering analysis **(a)** and ECs calculated individually for each region **(b)**. In **(a)**, black markers identify shrub fires belonging to clusters with less than 100 observations. In **(b)**, the mean shrubland biome EC is indicated by the black line, while the range of all mean biome ECs (as presented in Table 2) is indicated in grey.

We do not fully understand the causes of the observed ecoregion-scale differences. It is possible that differences in fuel N content and/or fire MCE are responsible, but evaluating these factors on the scale of an ecoregion requires an in-depth understanding of local fire behavior as well as observations of these factors that currently do not exist on the spatial or temporal scale of this analysis. Rather than speculating on specific causes here, we instead hope that identification of clear differences in different ecoregions guides future efforts to reveal and assess processes that govern fire emissions.

5.2 Comparison to previous work

We compare both to our previous work quantifying fire emissions from space, and to global biome EFs from conventional fire emission schemes.

5.2.1 California and Nevada revisited

In Mebust et al. (2011) we applied the same basic methodology with minor differences to fires over California and Nevada (126–113° W, 31–44° N) and found that our calculated MER was correlated with FRP with R^2 ranging from 0.3 to 0.8, that relative differences in emissions between fuel types previously obtained by in situ measurements were reproduced by our analysis, and that the absolute values of the ECs and EFs we measured were several times smaller than previously obtained EF and EC measurements. In this work, we update our analysis to incorporate a more recent version of the OMI NO_2 retrieval (Standard Product v2.1 vs. v1.0), a different wind dataset (CFSR winds at 850 hPa and 0.5° × 0.5° resolution vs. NARR winds at 900 hPa and 32 km resolution), additional years of observations (2009–2011), removal of OMI pixels containing less than 250 MW of total FRP from further analysis, and adjustments to how observations were selected for removal with respect to e.g. background, clear time, etc. Here we include a comparison to those previous results.

Figure 7 shows MER vs. FRP for (a) all fires, (b) forest fires, (c) shrub fires and (d) grass fires in the California/Nevada region indicated above, using the updated method. In most cases, the R^2 for each category is slightly higher than observed in Mebust et al. (2011), possibly due to improvements in methodology, improvements to the NO_2

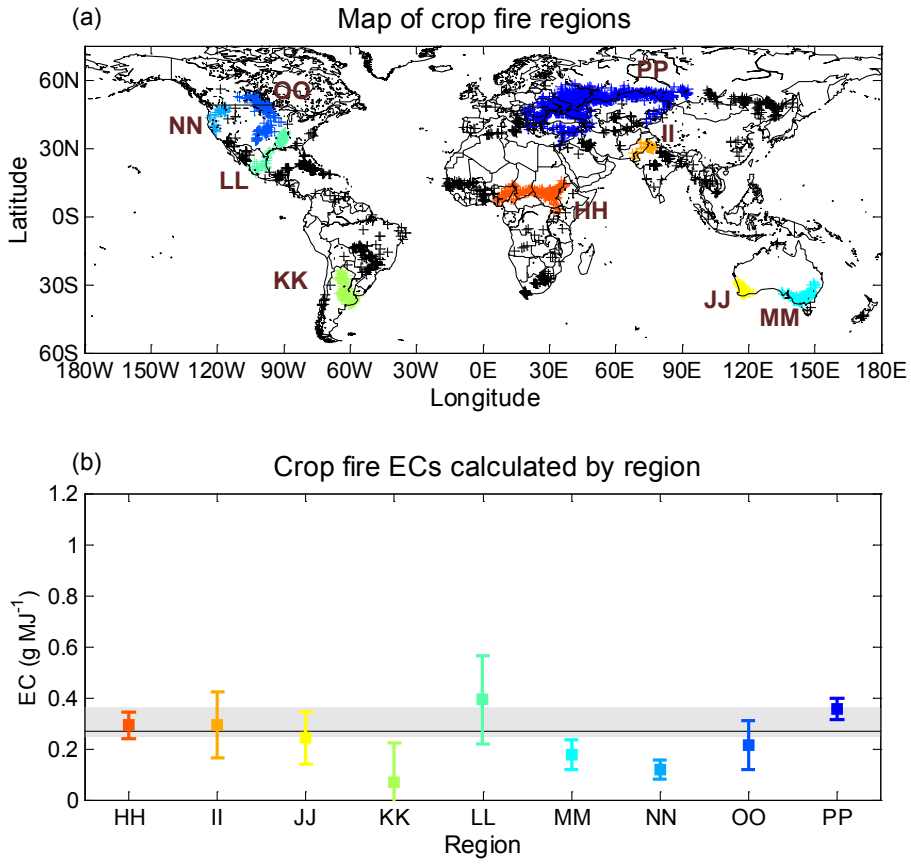

Fig. 6. A map of agricultural fire regions determined by a clustering analysis **(a)** and ECs calculated individually for each region **(b)**. In **(a)**, black markers identify agricultural fires belonging to clusters with less than 100 observations. In **(b)**, the mean agricultural biome EC is indicated by the black line, while the range of all mean biome ECs (as presented in Table 2) is indicated in grey.

retrieval in the Standard Product v2.1 vs. v1.0, and/or a reduction in the number of points scattered around zero. We also perform a multiple regression as in Mebust et al. (2011), and derive ECs of 0.203 ± 0.042, 0.290 ± 0.040, and 0.195 ± 0.022 g NO_x MJ^{-1} (as NO) for forest, shrub, and grass fires, respectively. In an absolute sense, these values are lower than those derived in Mebust et al. (2011) by 52 % for shrubs, 34 % for grasses, and 16 % for forests. Much of the decrease is due to generally lower values of tropospheric NO_2 columns in version 2.1 of the NASA OMNO2 standard product relative to version 1.0. Further reduction in the case of shrub fires is due to inclusion of the years 2009–2011 which had generally lower ECs ($\sim$ 26 % below the mean EC for all years).

In Mebust et al. (2011) we found that the relative differences between grass, shrub and forest fire ECs derived from OMI and MODIS data reproduced similar relative differences in EFs measured for primarily North American fires in situ. In this analysis, we find that the relative differences in ECs and EFs remain within one standard deviation of one another, though the agreement in the ratio is slightly worse. For example, the ratio of grass to forest fire EFs obtained in Battye and Battye (2002) is 1.4 ± 0.8; the ratio of ECs for the same fuels as reported in Mebust et al. (2011) is 1.2 ± 0.4 and in this work is 1.0 ± 0.2. The ratio between shrub and forest fire ECs in both studies is similarly within one standard deviation of the ratio of shrub and forest fire EFs. As in both Battye and Battye (2002) and Mebust et al. (2011), we find that shrub fires in this region emit more NO_x per unit energy (or mass) than either grass or forest fires. The reason for higher shrub NO_x emissions is unclear, but may stem from higher MCE, or from N deposition due to nearby anthropogenic emissions, an effect that is lessened in our analysis due to our removal of points with high NO_x background (Laursen et al., 1992). In both this work and Mebust et al. (2011), we find that forest ECs are higher (relative to grass and shrub fires) than EFs presented in Battye and Battye (2002).

5.2.2 Comparison with global EF summaries

There exist several previously published EFs intended for use in global models: an initial comprehensive summary of EFs for many species and fuel types presented by Andreae and Merlet (2001); two updates to that work (Hoelzemann

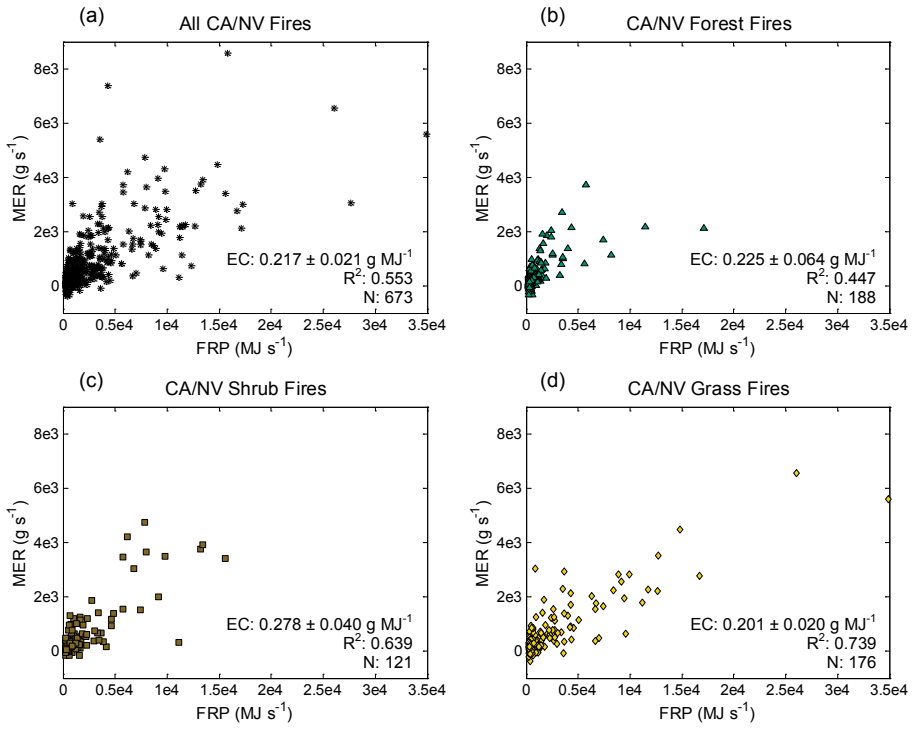

Fig. 7. Regressions of fire radiative power (FRP) vs. mass emission rate (MER) for **(a)** all fires, **(b)** forest fires, **(c)** shrub fires and **(d)** grass fires in the California/Nevada region (126–113° W, 31–44° N). Listed on each plot are the calculated EC (i.e. the slope of the best fit line), R^2, and number of points.

et al., 2004; van der Werf et al., 2010); and a recent summary using a more selective set of observations (Akagi et al., 2011). EFs from each of these references, along with ECs from this work, are shown in Fig. 8 (on different y axes). Values for temperate forest, extratropical forest and chaparral from Akagi et al. (2011) are updated to include observations that were published after the summary (Akagi et al., 2013; Yokelson et al., 2013); these updates are available at http://bai.acd.ucar.edu/Data/fire/. We note that EFs in previous studies are derived as the mean of several measurements, and the associated "error" bars shown in Fig. 8 are one standard deviation of the measurements. As we previously discussed, this means they reflect some of the natural variability in individual fire emissions, and are not an estimate of the uncertainty in the mean EF. This uncertainty could be estimated using the number of fires from which the EFs are derived, but this information is not easily and uniformly accessible and so we do not attempt it. The error bars for our work in Fig. 8 are estimates of the uncertainty in the EC, not the variance in individual measurements, and so they estimate a different quantity than the "error" bars from the other studies and should not be directly compared.

The previously published summaries differ substantially from one another, a reflection of the large variability in measured NO_x EFs for individual fires even within a single global-scale biome, and the relatively small sample size which results in substantial changes to the mean when new measurements are added. We find that our biome-scale ECs fall within a narrower range than all of the previous studies. In a relative sense, our values compare best with those updated from Akagi et al. (2011), although in forested regions they are generally higher (relative to other biomes). This difference may reflect the improvements in sampling coverage in the full satellite record vs. fire emissions measured in situ. However, it is also plausible that this difference results from a low bias in FRP over forested regions. Lower FRP in forest biomes due to canopy screening effects would elevate the ECs in those biomes relative to the other biomes. We estimate the plausible magnitude of this bias by assuming that the observed difference results entirely from the bias and not from sampling differences; in that case, FRP is biased low by $\sim 34\,\%$, $\sim 40\,\%$, and $\sim 67\,\%$ for tropical, temperate, and boreal forest fires, respectively. The difference in bias for boreal forest (vs. tropical and temperate forest) could be due to a higher proportion of burning of ground-level or below-ground burning (e.g. peat) in boreal fires. While the differences we observe relative to Akagi et al. (2011) are almost certainly varied in source, this nevertheless provides a rough estimate of one plausible bias. We note that this estimate is specific to the accuracy of FRP as it pertains to actively detected fires, not the accuracy of FRP at e.g. $0.5° \times 0.5°$

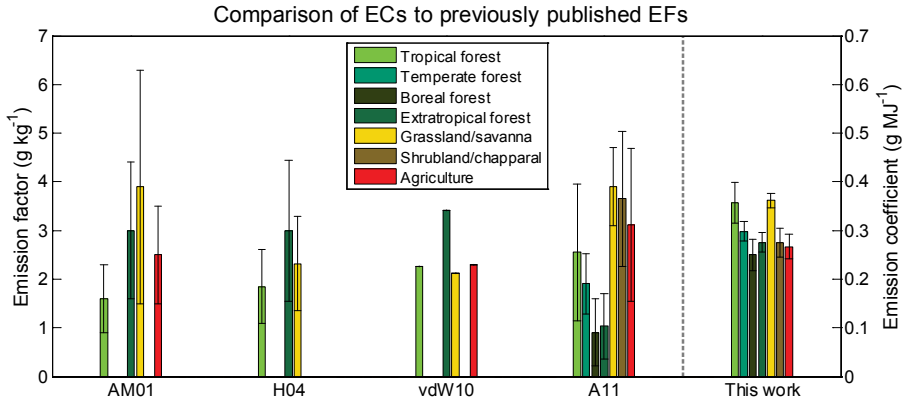

Fig. 8. Bar graph showing the different EFs (left *y* axis) in previous work and ECs (right *y* axis) presented here at the global biome scale. EFs from previous studies (from left to right) are: Andreae and Merlet (2001), Hoelzemann et al. (2004), van der Werf et al. (2010), Akagi et al. (2011). In previous work, error bars indicate one standard deviation of the mean; in the case of van der Werf et al. (2010), no standard deviation was reported. Error bars for this work indicate the standard error of the fit.

scale where canopy cover might completely obscure fires that would otherwise be detected by the MODIS algorithm.

Detailed information on the EF calculations in Akagi et al. (2011) is available in supplementary material of that paper, and thus we can directly compare regional differences in ECs presented here with the EFs used in Akagi et al. (2011) to examine how consistent our results are beyond broad biome categorizations. Akagi et al. (2011) divide the tropical forest NO_x EF into two EFs: one for tropical evergreen deforestation, and one for tropical dry deforestation that is approximately twice as high. When we calculate ECs separately for forest fires in "monsoonal" and "winter-dry" equatorial regimes, that value is higher (by a factor of 1.89) than the EC calculated for forest fires in the "fully humid" equatorial regime. If these climate classifications provide an adequate proxy for evergreen vs. dry deforestation, this result is consistent with Akagi et al. (2011). We also find that the temperate forest EC from Region J is very slightly below the mean temperate forest EC, and forest fire ECs in the California/Nevada region are even lower than in Region J; this is consistent with results from Akagi et al. (2011) in that measurements of California pine understory EFs made by Burling et al. (2011) are slightly below the mean temperate forest understory EF, and EFs from Oregon wildfires measured by Radke et al. (1991) are below the mean temperate forest EF.

In contrast, in Akagi et al. (2011) EFs reported for tropical forest fires in Mexico (Yokelson et al., 2011) are higher (3–5 g NO_x as NO kg^{-1}) on average than EFs for tropical forest fires in Brazil (1–2 g NO_x as NO kg^{-1}; Ferek et al., 1998; Yokelson et al., 2008), while our analysis suggests that ECs from tropical forests in Mexico and Brazil are similar to each other, with ECs in Mexico slightly lower (see Fig. 3, regions D and E). We also find that ECs for the region that encompasses North and South Carolina in our analysis (region G) are much higher than the mean EC for temperate forests, which is inconsistent with the below-mean (Akagi et al., 2013) or slightly above mean (Burling et al., 2011) EFs in the aggregate EF from Akagi et al. (2011) for this biome.

6 Conclusions

We present biome- and ecosystem-resolved NO_x ECs, based on satellite measurements of tropospheric NO_2 from OMI and of FRP from MODIS, for several different biome and ecosystem categories. These ECs are obtained via a method that was adapted from Mebust et al. (2011) for application to global fires and is also updated to include subsequent years of observations and an improved version of the OMI NO_2 retrieval. We compare our biome-scale ECs with summaries of EFs based on in situ measurements and find that the range of biome-scale ECs observed here is smaller than for EFs in previous works. Our results are for the most part consistent with relative differences in EFs from Akagi et al. (2011) although emissions in forest biomes are relatively higher.

We find that the majority of ecoregion-scale ECs are not statistically significantly different from the corresponding mean biome EC, while biome-scale ECs themselves fall into a narrow range with the smallest EC (0.250 g MJ^{-1}) fully 70 % of the largest (0.362 g MJ^{-1}) EC. We do, however, observe ecoregion-scale ECs that are both significantly and substantially different from the mean biome EC and/or from the range of biome-scale ECs, demonstrating that there exist regions where mean fire NO_x emission behavior is very different from the global mean. While mean biome and ecoregion ECs are relatively similar, variability in individual fire ECs remains high. Future efforts should focus on elucidating the particular processes that govern this variability; the observed differences in ECs can hopefully guide these efforts by identifying regions where there are important differences in fire NO_x emission behavior.

Supplementary material related to this article is available online at http://www.atmos-chem-phys.net/14/2509/2014/acp-14-2509-2014-supplement.zip.

Acknowledgements. This work was supported by the National Aeronautics and Space Administration, grants NNX08AE566 and NNX12AB79G, and by the Department of Energy Office of Science Graduate Fellowship Program (DOE SCGF), made possible in part by the American Recovery and Reinvestment Act of 2009, administered by ORISE-ORAU under contract no. DE-AC05-06OR23100. All opinions expressed in this paper are the authors' and do not necessarily reflect the policies and views of DOE, ORAU, or ORISE. OMI data used in this effort were acquired as part of the activities of NASA's Science Mission Directorate, and are archived and distributed by the Goddard Earth Sciences Data and Information Services Center at http://disc.sci.gsfc.nasa.gov/Aura/data-holdings/OMI/omno2_v003.shtml. MODIS data are distributed by the Land Processes Distributed Active Archive Center, located at the U.S. Geological Survey Earth Resources Observation and Science Center (http://lpdaac.usgs.gov). CFSR and CFSv2 data were obtained through the National Center for Atmospheric Research Computer and Information Systems Laboratory Research Data Archive (http://rda.ucar.edu/). Köppen-Geigeer climate classification data are available at available at http://koeppen-geiger.vu-wien.ac.at/present.htm. We thank S. Akagi for providing additional information regarding EFs published in Akagi et al. (2011).

Edited by: P. O. Wennberg

References

Akagi, S. K., Yokelson, R. J., Wiedinmyer, C., Alvarado, M. J., Reid, J. S., Karl, T., Crounse, J. D., and Wennberg, P. O.: Emission factors for open and domestic biomass burning for use in atmospheric models, Atmos. Chem. Phys., 11, 4039–4072, doi:10.5194/acp-11-4039-2011, 2011.

Akagi, S. K., Yokelson, R. J., Burling, I. R., Meinardi, S., Simpson, I., Blake, D. R., McMeeking, G. R., Sullivan, A., Lee, T., Kreidenweis, S., Urbanski, S., Reardon, J., Griffith, D. W. T., Johnson, T. J., and Weise, D. R.: Measurements of reactive trace gases and variable O_3 formation rates in some South Carolina biomass burning plumes, Atmos. Chem. Phys., 13, 1141–1165, doi:10.5194/acp-13-1141-2013, 2013.

Andreae, M. O. and Merlet, P.: Emission of trace gases and aerosols from biomass burning, Global Biogeochem. Cy., 15, 955–966, 2001.

Battye, W. and Battye, R.: Development of emissions inventory methods for wildland fire, US Environmental Protection Agency, Research Triangle Park, N.C., Contract 68-D-98-046, 2002.

Boersma, K. F., Bucsela, E., Brinksma, E., and Gleason, J. F.: NO_2, in: OMI Algorithm Theoretical Basis Document, Volume IV: OMI Trace Gas Algorithms, 2 Edn., edited by: Chance, K., Smithsonian Astrophysical Observatory, Cambridge, MA, 13–36, 2002.

Boersma, K. F., Eskes, H. J., Dirksen, R. J., van der A, R. J., Veefkind, J. P., Stammes, P., Huijnen, V., Kleipool, Q. L., Sneep, M., Claas, J., Leitão, J., Richter, A., Zhou, Y., and Brunner, D.: An improved tropospheric NO_2 column retrieval algorithm for the Ozone Monitoring Instrument, Atmos. Meas. Tech., 4, 1905–1928, doi:10.5194/amt-4-1905-2011, 2011.

Boschetti, L. and Roy, D. P.: Strategies for the fusion of satellite fire radiative power with burned area data for fire radiative energy derivation, J. Geophys. Res.-Atmos., 114, D20302, doi:10.1029/2008JD011645, 2009.

Bowman, D. M. J. S., Balch, J. K., Artaxo, P., Bond, W. J., Carlson, J. M., Cochrane, M. A., D'Antonio, C. M., DeFries, R. S., Doyle, J. C., Harrison, S. P., Johnston, F. H., Keeley, J. E., Krawchuk, M. A., Kull, C. A., Marston, J. B., Moritz, M. A., Prentice, I. C., Roos, C. I., Scott, A. C., Swetnam, T. W., van der Werf, G. R., and Pyne, S. J.: Fire in the Earth System, Science, 324, 481–484, 2009.

Bucsela, E. J., Krotkov, N. A., Celarier, E. A., Lamsal, L. N., Swartz, W. H., Bhartia, P. K., Boersma, K. F., Veefkind, J. P., Gleason, J. F., and Pickering, K. E.: A new stratospheric and tropospheric NO_2 retrieval algorithm for nadir-viewing satellite instruments: applications to OMI, Atmos. Meas. Tech. Discuss., 6, 1361–1407, doi:10.5194/amtd-6-1361-2013, 2013.

Burling, I. R., Yokelson, R. J., Akagi, S. K., Urbanski, S. P., Wold, C. E., Griffith, D. W. T., Johnson, T. J., Reardon, J., and Weise, D. R.: Airborne and ground-based measurements of the trace gases and particles emitted by prescribed fires in the United States, Atmos. Chem. Phys., 11, 12197–12216, doi:10.5194/acp-11-12197-2011, 2011.

Efron, B. and Tibshirani, R.: Bootstrap Methods for Standard Errors, Confidence Intervals, and Other Measures of Statistical Accuracy, Stat. Sci., 1, 54–75, 1986.

Ferek, R. J., Reid, J. S., Hobbs, P. V., Blake, D. R., and Liousse, C.: Emission factors of hydrocarbons, halocarbons, trace gases and particles from biomass burning in Brazil, J. Geophys. Res.-Atmos., 103, 32107–32118, 1998.

Fiore, A. M., Naik, V., Spracklen, D. V., Steiner, A., Unger, N., Prather, M., Bergmann, D., Cameron-Smith, P. J., Cionni, I., Collins, W. J., Dalsoren, S., Eyring, V., Folberth, G. A., Ginoux, P., Horowitz, L. W., Josse, B., Lamarque, J. F., MacKenzie, I. A., Nagashima, T., O'Connor, F. M., Righi, M., Rumbold, S. T., Shindell, D. T., Skeie, R. B., Sudo, K., Szopa, S., Takemura, T., and Zeng, G.: Global air quality and climate, Chem. Soc. Rev., 41, 6663–6683, 2012.

Freeborn, P. H., Wooster, M. J., Hao, W. M., Ryan, C. A., Nordgren, B. L., Baker, S. P., and Ichoku, C.: Relationships between energy release, fuel mass loss, and trace gas and aerosol emissions during laboratory biomass fires, J. Geophys. Res., 113, D01301, doi:10.1029/2007JD008679, 2008.

Freeborn, P. H., Wooster, M. J., and Roberts, G.: Addressing the spatiotemporal sampling design of MODIS to provide estimates of the fire radiative energy emitted from Africa, Remote Sens. Environ., 115, 475–489, 2011.

Friedl, M. A., Sulla-Menashe, D., Tan, B., Schneider, A., Ramankutty, N., Sibley, A., and Huang, X. M.: MODIS Collection 5 global land cover: Algorithm refinements and characterization of new datasets, Remote Sens. Environ., 114, 168–182, 2010.

Giglio, L., Descloitres, J., Justice, C. O., and Kaufman, Y. J.: An enhanced contextual fire detection algorithm for MODIS, Remote Sens. Environ., 87, 273–282, 2003.

Granier, C., Bessagnet, B., Bond, T., D'Angiola, A., van der Gon, H. D., Frost, G. J., Heil, A., Kaiser, J. W., Kinne, S., Klimont, Z., Kloster, S., Lamarque, J. F., Liousse, C., Masui, T., Meleux, F., Mieville, A., Ohara, T., Raut, J. C., Riahi, K., Schultz, M. G., Smith, S. J., Thompson, A., van Aardenne, J., van der Werf, G. R., and van Vuuren, D. P.: Evolution of anthropogenic and biomass burning emissions of air pollutants at global and regional scales during the 1980–2010 period, Clim. Change, 109, 163–190, 2011.

Hoelzemann, J. J., Schultz, M. G., Brasseur, G. P., Granier, C., and Simon, M.: Global Wildland Fire Emission Model (GWEM): Evaluating the use of global area burnt satellite data, J. Geophys. Res., 109, D14S04, doi:10.1029/2003JD003666, 2004.

Ichoku, C. and Kaufman, Y. J.: A method to derive smoke emission rates from MODIS fire radiative energy measurements, IEEE T. Geosci. Remote, 43, 2636–2649, 2005.

Jacob, D. J., Crawford, J. H., Maring, H., Clarke, A. D., Dibb, J. E., Emmons, L. K., Ferrare, R. A., Hostetler, C. A., Russell, P. B., Singh, H. B., Thompson, A. M., Shaw, G. E., McCauley, E., Pederson, J. R., and Fisher, J. A.: The Arctic Research of the Composition of the Troposphere from Aircraft and Satellites (ARCTAS) mission: design, execution, and first results, Atmos. Chem. Phys., 10, 5191–5212, doi:10.5194/acp-10-5191-2010, 2010.

Jaffe, D. A. and Wigder, N. L.: Ozone production from wildfires: A critical review, Atmos. Environ., 51, 1–10, 2012.

Jordan, N. S., Ichoku, C., and Hoff, R. M.: Estimating smoke emissions over the US Southern Great Plains using MODIS fire radiative power and aerosol observations, Atmos. Environ., 42, 2007–2022, 2008.

Justice, C. O., Giglio, L., Korontzi, S., Owens, J., Morisette, J. T., Roy, D., Descloitres, J., Alleaume, S., Petitcolin, F., and Kaufman, Y.: The MODIS fire products, Remote Sens. Environ., 83, 244–262, 2002.

Kaufman, Y. J., Justice, C. O., Flynn, L. P., Kendall, J. D., Prins, E. M., Giglio, L., Ward, D. E., Menzel, W. P., and Setzer, A. W.: Potential global fire monitoring from EOS-MODIS, J. Geophys. Res., 103, 32215–32238, 1998.

Korontzi, S., Ward, D. E., Susott, R. A., Yokelson, R. J., Justice, C. O., Hobbs, P. V., Smithwick, E. A. H., and Hao, W. M.: Seasonal variation and ecosystem dependence of emission factors for selected trace gases and $PM_{2.5}$ for southern African savanna fires, J. Geophys. Res., 108, 4758, doi:10.1029/2003JD003730, 2003.

Kottek, M., Grieser, J., Beck, C., Rudolf, B., and Rubel, F.: World map of the Koppen-Geiger climate classification updated, Meteorol. Z., 15, 259–263, 2006.

Lacaux, J. P., Delmas, R., Jambert, C., and Kuhlbusch, T. A. J.: NO_x emissions from African savanna fires, J. Geophys. Res., 101, 23585–23595, 1996.

Laursen, K. K., Hobbs, P. V., Radke, L. F., and Rasmussen, R. A.: Some trace gas emissions from North American biomass fires with an assessment of regional and global fluxes from biomass burning, J. Geophys. Res., 97, 20687–20701, 1992.

Leitão, J., Richter, A., Vrekoussis, M., Kokhanovsky, A., Zhang, Q. J., Beekmann, M., and Burrows, J. P.: On the improvement of NO_2 satellite retrievals – aerosol impact on the airmass factors, Atmos. Meas. Tech., 3, 475–493, doi:10.5194/amt-3-475-2010, 2010.

Mebust, A. K. and Cohen, R. C.: Observations of a seasonal cycle in NO_x emissions from fires in African woody savannas, Geophys. Res. Lett., 40, 1451–1455, 2013.

Mebust, A. K., Russell, A. R., Hudman, R. C., Valin, L. C., and Cohen, R. C.: Characterization of wildfire NO_x emissions using MODIS fire radiative power and OMI tropospheric NO_2 columns, Atmos. Chem. Phys., 11, 5839–5851, doi:10.5194/acp-11-5839-2011, 2011.

Monfreda, C., Ramankutty, N., and Foley, J. A.: Farming the planet: 2. Geographic distribution of crop areas, yields, physiological types, and net primary production in the year 2000, Global Biogeochem. Cy., 22, GB1022, doi:10.1029/2007GB002947, 2008.

Radke, L. F., Hegg, D. A., Hobbs, P. V., Nance, J. D., Lyons, J. H., Laursen, K. K., Weiss, R. E., Riggan, P. J., and Ward, D. E.: Particulate and trace gas emissions from large biomass fires in North America, in: Global biomass burning – Atmospheric, climatic, and biospheric implications, MIT Press, Cambridge, MA, 209–224, 1991.

Russell, A. R., Perring, A. E., Valin, L. C., Bucsela, E. J., Browne, E. C., Wooldridge, P. J., and Cohen, R. C.: A high spatial resolution retrieval of NO_2 column densities from OMI: method and evaluation, Atmos. Chem. Phys., 11, 8543–8554, doi:10.5194/acp-11-8543-2011, 2011.

Saha, S., Moorthi, S., Pan, H. L., Wu, X. R., Wang, J. D., Nadiga, S., Tripp, P., Kistler, R., Woollen, J., Behringer, D., Liu, H. X., Stokes, D., Grumbine, R., Gayno, G., Wang, J., Hou, Y. T., Chuang, H. Y., Juang, H. M. H., Sela, J., Iredell, M., Treadon, R., Kleist, D., Van Delst, P., Keyser, D., Derber, J., Ek, M., Meng, J., Wei, H. L., Yang, R. Q., Lord, S., Van den Dool, H., Kumar, A., Wang, W. Q., Long, C., Chelliah, M., Xue, Y., Huang, B. Y., Schemm, J. K., Ebisuzaki, W., Lin, R., Xie, P. P., Chen, M. Y., Zhou, S. T., Higgins, W., Zou, C. Z., Liu, Q. H., Chen, Y., Han, Y., Cucurull, L., Reynolds, R. W., Rutledge, G., and Goldberg, M.: The NCEP Climate Forecast System Reanalysis, B. Am. Meteorol. Soc., 91, 1015–1057, 2010.

Saha, S., Moorthi, S., Wu, X., Wang, J., Nadiga, S., Tripp, P., Behringer, D., Hou, Y.-T., Chuang, H.-y., Iredell, M., Ek, M., Meng, J., Yang, R., Mendez, M. P., Dool, H. v. d., Zhang, Q., Wang, W., Chen, M., and Becker, E.: The NCEP Climate Forecast System Version 2, J. Climate, doi:10.1175/JCLI-D-12-00823.1, 2014.

Simpson, I. J., Akagi, S. K., Barletta, B., Blake, N. J., Choi, Y., Diskin, G. S., Fried, A., Fuelberg, H. E., Meinardi, S., Rowland, F. S., Vay, S. A., Weinheimer, A. J., Wennberg, P. O., Wiebring, P., Wisthaler, A., Yang, M., Yokelson, R. J., and Blake, D. R.: Boreal forest fire emissions in fresh Canadian smoke plumes: C_1–C_{10} volatile organic compounds (VOCs), CO_2, CO, NO_2, NO, HCN and CH_3CN, Atmos. Chem. Phys., 11, 6445–6463, doi:10.5194/acp-11-6445-2011, 2011.

van der Werf, G. R., Randerson, J. T., Giglio, L., Collatz, G. J., Mu, M., Kasibhatla, P. S., Morton, D. C., DeFries, R. S., Jin, Y., and van Leeuwen, T. T.: Global fire emissions and the contribution of deforestation, savanna, forest, agricultural, and peat fires (1997–2009), Atmos. Chem. Phys., 10, 11707–11735, doi:10.5194/acp-10-11707-2010, 2010.

van Leeuwen, T. T. and van der Werf, G. R.: Spatial and temporal variability in the ratio of trace gases emitted from biomass

burning, Atmos. Chem. Phys., 11, 3611–3629, doi:10.5194/acp-11-3611-2011, 2011.

van Leeuwen, T. T., Peters, W., Krol, M. C., and van der Werf, G. R.: Dynamic biomass burning emission factors and their impact on atmospheric CO mixing ratios, J. Geophys. Res.-Atmos., 118, 6797–6815, doi:10.1002/jgrd.50478, 2013.

Vermote, E., Ellicott, E., Dubovik, O., Lapyonok, T., Chin, M., Giglio, L., and Roberts, G. J.: An approach to estimate global biomass burning emissions of organic and black carbon from MODIS fire radiative power, J. Geophys. Res., 114, D18205, doi:10.1029/2008JD011188, 2009.

Wiedinmyer, C., Quayle, B., Geron, C., Belote, A., McKenzie, D., Zhang, X. Y., O'Neill, S., and Wynne, K. K.: Estimating emissions from fires in North America for air quality modeling, Atmos. Environ., 40, 3419–3432, 2006.

Wooster, M. J.: Small-scale experimental testing of fire radiative energy for quantifying mass combusted in natural vegetation fires, Geophys. Res. Lett., 29, 2027, doi:2010.1029/2002GL015487, 2002.

Wooster, M. J., Zhukov, B., and Oertel, D.: Fire radiative energy for quantitative study of biomass burning: derivation from the BIRD experimental satellite and comparison to MODIS fire products, Remote Sens. Environ., 86, 83–107, 2003.

Wooster, M. J., Roberts, G., Perry, G. L. W., and Kaufman, Y. J.: Retrieval of biomass combustion rates and totals from fire radiative power observations: FRP derivation and calibration relationships between biomass consumption and fire radiative energy release, J. Geophys. Res., 110, D24311, doi:10.1029/2005JD006318, 2005.

Yokelson, R. J., Christian, T. J., Karl, T. G., and Guenther, A.: The tropical forest and fire emissions experiment: laboratory fire measurements and synthesis of campaign data, Atmos. Chem. Phys., 8, 3509–3527, doi:10.5194/acp-8-3509-2008, 2008.

Yokelson, R. J., Burling, I. R., Urbanski, S. P., Atlas, E. L., Adachi, K., Buseck, P. R., Wiedinmyer, C., Akagi, S. K., Toohey, D. W., and Wold, C. E.: Trace gas and particle emissions from open biomass burning in Mexico, Atmos. Chem. Phys., 11, 6787–6808, doi:10.5194/acp-11-6787-2011, 2011.

Yokelson, R. J., Burling, I. R., Gilman, J. B., Warneke, C., Stockwell, C. E., de Gouw, J., Akagi, S. K., Urbanski, S. P., Veres, P., Roberts, J. M., Kuster, W. C., Reardon, J., Griffith, D. W. T., Johnson, T. J., Hosseini, S., Miller, J. W., Cocker III, D. R., Jung, H., and Weise, D. R.: Coupling field and laboratory measurements to estimate the emission factors of identified and unidentified trace gases for prescribed fires, Atmos. Chem. Phys., 13, 89–116, doi:10.5194/acp-13-89-2013, 2013.